Analysis of the differential secretome of nasopharyngeal carcinoma cell lines CNE-2R and CNE-2

ZE-TAN CHEN[1,2], LING LI[1,2], YA GUO[3], SONG QU[1,2], WEI ZHAO[1,2], HAO CHEN[1,2], FANG SU[1,2], JUN YIN[1,2], QI-YAN MO[1,2] and XIAO-DONG ZHU[1,2]

[1]Department of Radiation Oncology, Cancer Hospital of Guangxi Medical University and Cancer Institute of Guangxi Zhuang Autonomous Region; [2]Key Laboratory of High-Incidence-Tumor Prevention and Treatment (Guangxi Medical University), Ministry of Education, Nanning, Guangxi 530021; [3]Department of Radiation Oncology, The Second Affiliated Hospital of Xi'an Jiaotong University, Xi'an, Shaanxi 710004, P.R. China

Received June 13, 2015; Accepted July 23, 2015

DOI: 10.3892/or.2015.4255

Abstract. Radioresistance is the major cause of poor prognosis in nasopharyngeal carcinoma (NPC). To identify and characterize the secretome associated with NPC radioresistance, we compared the conditioned serum-free medium of radioresistant CNE-2R cells with that of the parental radiosensitive CNE-2 cells using isobaric tags for relative and absolute quantitation (iTRAQ) with liquid chromatography-electrospray tandem mass spectrometry (LC-ESI-MS/MS) quantitative proteomics. Before proceeding to quantitative proteomics, we investigated the survival curves of CNE-2R and CNE-2 cells by colony formation assay, and the CNE-2R survival curves were significantly higher than those for CNE-2. In total, 3,581 proteins were identified in the quantitative proteomics experiments, and 40 proteins exhibited significant differences between the CNE-2R and CNE-2 cells. Twenty-six of the 40 proteins were secreted by classical, non-classical, or exosomal secretion pathways. To verify the reliability of iTRAQ quantitative proteomics, we applied western blotting (WB) to study the secretory protein expression of fibrillin-2, CD166, sulfhydryl oxidase 1 and cofilin-2, which are involved in cell adhesion, migration and invasion. The WB results showed that fibrillin-2 (p=0.017) and sulfhydryl oxidase 1 (p=0.000) were highly expressed in the CNE-2 cells, while CD166 (p=0.012) and cofilin-2 (p=0.003) were highly expressed in the CNE-2R cells, which was in accordance with iTRAQ quantitative proteomics. Finally, a phenotypic subset of CD166-positive NPC cells was verified by immunocytochemistry. In summary, we defined a collection of secretory proteins that may be relevant to the radioresistance in NPC cells, and we determined that CD166, which is widely used as a positive marker of cancer stem cells, is expressed in NPC cells.

Correspondence to: Professor Xiao-Dong Zhu, Department of Radiation Oncology, Cancer Hospital of Guangxi Medical University and Cancer Institute of Guangxi Zhuang Autonomous Region, 71 He Di Road, Nanning, Guangxi 530021, P.R. China
E-mail: zhuxdonggxmu@126.com

Key words: CD166, cancer stem cells, cofilin-2, fibrillin-2, nasopharyngeal carcinoma, secretome

Introduction

Nasopharyngeal carcinoma (NPC) is a highly malignant carcinoma characterized by local invasion and early distant metastasis (1). NPC is endemic in regions such as Southeast Asia, Southern China, Hong Kong and Taiwan, where the annual incidence rate is ~25-fold higher than that in the Western world (2-4). Radiotherapy is the main treatment for NPC. During the past decades, there have been advances in radiotherapy techniques, dose escalation and the use of chemotherapy; however, ~20% of NPC patients have local recurrence following radiation, and a common cause of local recurrence with poor survival in NPC is radioresistance (5,6). Therefore, identifying molecules secreted from the NPC environment into the body fluid that could be used as clinically predictive biomarkers for radioresistance is vital. Knowing the biomarkers for radioresistance and modifying the therapeutic approach individually will be important in mitigating NPC disease burden and mortality.

Proteomic approaches have been widely used for the analysis of malignant diseases, particularly in the field of plasma/serum tumor marker identification (7-10). Thus, the topic of NPC proteomics has been analyzed in numerous studies over the past decade. For example, Juan *et al* (11) used a xenotransplantation model to explore tumor-associated serum proteins derived from mouse or human origin through their separation and identification by 2-dimensional gel electrophoresis (2-DE) and mass spectrometry (MS), finding that a panel of proteins serves as screening biomarkers for early cancer detection. Wu *et al* (12,13) in 2005 and 2008 used MS to identify secreted proteomes in early NPC diagnosis and showed that the proteins fibronectin, Mac-2 BP, PAI-1 and Prx-II may be potential markers for the diagnosis of NPC. In addition, Chang *et al* (14) identified candidate NPC serum biomarkers via cancer cell secretome and tissue transcriptome analysis, finding that serum levels of cystatin A, cathepsin B, manganese superoxide dismutase and matrix metalloproteinase 2 were higher in NPC patients than these

levels in healthy controls. However, these strategies were limited, as the mouse xenotransplantation model and human body fluid all had individual limitations. Use of the mouse xenotransplantation model was aborted due to substantial mouse protein content, and human body fluid was limited due to its formidable heterogenicity. Thus, cell lines were considered to be more valuable in proteomic studies due to their low complexity and variability of proteins with which to explore NPC-related proteins (15).

CNE-2 is a low-differentiated NPC epithelioid cell line derived from a primary tumor biopsy in China in 1980 (16). Its establishment has been applied to a multitude of NPC-related studies. For example, Li *et al* (17) combined 2-DE with MALDI-TOF MS for analysis of the proteins in CNE-2 cells and its strongly metastatic subclone S-18 and for the functional characterization of HSP27 in the metastasis of NPC. CNE-2R, a radioresistant NPC cell line, was established from CNE-2 cells that had undergone 400 cGy ^{60}Co γ-radiation repeated 16 times for a total dose of 64 Gy for 1 year (18). The isobaric tags for relative and absolute quantitation (iTRAQ) approach is a gel-free labeling method for use in complex samples, and is currently the main approach in quantitative proteomic analysis. This scenario is complemented by the in-gel labeling method of classic 2-DE analysis (19). Herein, we applied iTRAQ quantitative proteomics to this experiment, a qualitative and quantitative analysis more accurate than traditional 2-DE that could prove truly beneficial to the understanding of radioresistance for nasopharyngeal carcinoma (20).

In the present study, we presented an investigation of the differential secretome associated with NPC radioresistance using the iTRAQ system and liquid chromatography-electrospray tandem mass spectrometry (LC-ESI-MS/MS). This approach allows the simultaneous comparison of multiple peptides via measuring the peak intensities of reporter ions in tandem MS/MS spectra (19). Finally, a collection of secretory proteins may provide a resource and strategy for the further investigation of NPC related to radioresistance.

Materials and methods

Cell culture. The CNE-2 cell line was purchased from the Cancer Hospital of Shanghai Fudan University. The radioresistant cell line CNE-2R was constructed by subjecting the CNE-2 cell line to fractionated radiation in our previous study (18). CNE-2 and CNE-2R cells were cultured in RPMI-1640 medium with the addition of 10% fetal bovine serum (FBS) (both from Gibco, USA), penicillin (100 U/ml) and streptomycin (100 μg/ml), and were cultured in a humidified 5% CO_2 atmosphere at 37˚C as previously described (21).

Colony formation assay for radiosensitivity. Aliquots consisting of 200, 200, 400, 600, 1,000, 5,000 and 10,000 CNE-2 and CNE-2R cells were plated into seven 6-well plates and individually exposed to doses of 0, 1, 2, 4, 6, 8 and 10 Gy with 6 MV X-rays from an Elekta linear accelerator (Precise 1120; Elekta Instrument AB, Stockholm, Sweden) with a dose rate of 220 cGy/min. After irradiation, the cells were cultured for 10 days in a 5% CO_2 atmosphere at 37˚C. The colonies were fixed with carbinol and stained with 0.1% Giemsa (both from Solarbio, Beijing, China). The number of surviving colonies (defined as any colony with ≥50 cells) was counted. All experiments were repeated 3 times. The dose responses were analyzed using a linear-quadratic relationship model (LQ model): ($y = \exp[-(\alpha x+\beta x^2)]$). The GraphPad Prism 5.0 software was used to create fit curves, where α and β are radiobiological parameters.

Cell cultures and preparation of conditioned media. CNE-2 and CNE-2R cells were seeded in ten 75 cm^2 culture flasks with 10 ml conditioned media each and cultured at 37˚C until the cells grew to 60-70% confluency (22,23). All cells were then washed 3 times with phosphate-buffered saline (PBS) to remove any adherent serum and cultured in RPMI-1640 phenol red-free medium without FBS (conditioned media) for 2 h. Afterwards, all cells were again washed 3 times with PBS to remove any adherent serum. All cells were then cultured in conditioned media for 24 h. Post starvation, the conditioned media from each cell line were collected and centrifuged at 1,000 x g for 10 min followed by 3,000 x g for 10 min to remove any cells or debris. The supernatant was filtered using a 0.22-μm filter, and one protease inhibitor tablet was added/50 ml (Complete Protease Inhibitor Cocktail; Roche, Mannheim, Germany). The supernatant was subsequently precipitated using acetone, then alkylated and the pellet was dissolved in 200 μl 0.5 M tetraethylammonium bromide (TEAB). The protein concentration was measured using the Branford assay kit (Pierce, Rockford, IL, USA). The proteins in the supernatant were stored at -80˚C for further analysis.

Trypan blue dye exclusion assay. Trypan blue dye exclusion assays and cell counting were used to determine viable cell numbers (24). CNE-2 and CNE-2R cells were seeded into 75 cm^2 culture flasks and cultured at 37˚C until the cells grew to 60-70% confluency. After washing 3 times with PBS, the cells were incubated in conditioned media for 2 h, then washed with PBS 3 times again and incubated in 10 ml conditioned media for 24 h. The supernatant and adherent cells from the CNE-2 and CNE-2R cell lines were quantified using the trypan blue exclusion method, where cells were diluted with 0.4% trypan blue dye (Sigma-Aldrich, St. Louis, MO, USA) in a 1:1 ratio and counted using a Neubauer hemocytometer under a phase-contrast microscope (IX71; Olympus, Beijing, China). The experiments were performed in triplicate.

SDS-PAGE. Based on the concentration results, 5 μg of protein samples from CNE-2 and CNE-2R cells was obtained and mixed briefly in equivalent loading buffer at 95˚C in a heat block for 5 min. One sample was loaded/well, in duplicate. Then, 12 μl of marker standard was loaded onto this gel, and electrophoresis was performed for 2 h at 120 V. The gel concentration was 10%. When electrophoresis was completed, the gel was dyed with dyeing buffer for 2 h and then destained using destaining buffer 3 times for 30 min each time.

Protein digestion, iTRAQ labeling and SCX chromatography. Total protein (100 μg) was obtained from the CNE-2 and CNE-2R solutions and digested with Trypsin Gold (Promega, Madison, WI, USA) at a protein:trypsin ratio of 30:1 at 37˚C for 16 h. After trypsin digestion, the peptides were dried by vacuum centrifugation, restored in 0.5 M TEAB and

processed according to the manufacturer's protocol for iTRAQ reagent (AB Sciex Inc., Foster City, CA, USA). In brief, one unit of iTRAQ reagent was thawed and reconstituted in 24 μl isopropanol. Peptides of the CNE-2 cell line were labeled with iTRAQ reagents 119 and 121, while CNE-2R peptides were labeled with 113 and 115. The peptides were incubated at room temperature for 2 h, pooled and dried by vacuum centrifugation. Finally, SCX chromatography was performed using an LC-20AB HPLC pump system (Shimadzu, Kyoto, Japan). The peptide mixtures were restored with 4 ml buffer A (25 mM NaH_2PO_4 in 25% ACN, pH 2.7) and loaded onto a 4.6x250 mm Ultramax SCX column containing 5-μm particles (Phenomenex, USA), which were eluted at a rate of 1 ml/min with a gradient of buffer A for 10 min, 5-60% buffer B (25 mM NaH_2PO_4, 1 M KCl in 25% ACN, pH 2.7) for 27 min and 60-100% buffer B for 1 min. Afterwards, the system was maintained in 100% buffer B for 1 min, and then equilibrated with buffer A for 10 min before the next injection. This elution process was monitored by measuring the absorbance at 214 nm, and fractions were collected every 1 min. The eluted peptides were pooled into a total of 20 fractions, desalted with a Strata-X-C18 column (Phenomenex) and vacuum-dried.

LC-ESI-MS/MS analysis based on TripleTOF 5600. Each fraction was resuspended in buffer A (5% ACN, 0.1% FA) and centrifuged at 20,000 x g for 10 min. The final concentration of peptide was 0.5 μg/μl on average. Next, 10 μl of the peptide supernatant was loaded on a 2-cm C18 trap column in an LC-20AD Nano HPLC (Shimadzu) by autosampler. Afterwards, the peptides were eluted onto a 10-cm analytical C18 column (inner diameter, 75 μm) packed in-house. The samples were then loaded at 8 μl/min for 4 min, and a 35-min gradient was run at 300 nl/min starting from 2 to 35% B (95% ACN, 0.1% FA), followed by a 5-min linear gradient to 60%, and then by a 2-min linear gradient to 80%, maintained at 80% B for 4 min, and finally returned to 5% in 1 min. Data were collected using a TripleTOF 5600 System fitted with a NanoSpray III source (AB Sciex, Concord, ON, Canada) and a pulled quartz tip as the emitter (New Objectives, Woburn, MA, USA), using an ion spray voltage of 2.5 kV, curtain gas of 30 psi, nebulizer gas of 15 psi, and an interface heater temperature of 150˚C. The MS was operated with RP ≥30,000 FWHM for TOF MS scans. For IDA, survey scans were obtained in 250 msec, and 30 product ion scans were collected if a threshold of 120 counts/sec was exceeded, with a 2+ to 5+ charge-state. The total cycle time was fixed to 3.3 sec. The Q2 transmission window was 100 Da for 100%. Four time bins were summed for each scan at a pulse frequency value of 11 kHz through monitoring of the 40 GHz multichannel TDC detector with four-anode channel ion detection. A sweeping collision energy setting of 35±5 eV coupled with iTRAQ adjusted rolling collision energy was applied to all precursor ions for collision-induced dissociation. Dynamic exclusion was set to 1/2 of peak width (15 sec), and the precursor was refreshed from the exclusion list.

Data analysis. Raw data files obtained from the Orbitrap were converted into MGF files using Proteome Discoverer 1.2 (PD 1.2; Thermo), (5600 MSConverter) and the MGF files were searched. Protein identification was performed using the Mascot 2.3.02 search engine (Matrix Science, London, UK) against a database containing 15,508 sequences. For protein identification, a mass tolerance of 0.05 Da was permitted for intact peptide masses and 0.1 Da for fragmented ions, with allowance for one missed cleavage in the trypsin digests. Gln->pyro-Glu (N-term Q), oxidation (M) and iTRAQ8plex (Y) were the potential variable modifications, and carbamidomethyl (C), iTRAQ 8-plex (N-term) and iTRAQ8-plex (K) were the fixed modifications. The charge states of peptides were set to +2 and +3. Specifically, an automatic decoy database search was run in Mascot by choosing the decoy checkbox, in which a random database sequence is generated and detected for raw spectra alongside the real database. To reduce the likelihood of false peptide identification, only peptides with significance scores greater than 'identity' (≥20) at the 99% confidence interval according to a Mascot 2.3.02 probability analysis were computed as identified. For every confidently identified protein, identification involved at least one unique peptide. For protein quantitation, it was necessary for a protein to contain at least two unique peptides. The quantitative protein ratio was weighted and normalized by the median ratio in Mascot 2.3.02. We considered ratios with p-values <0.05 and fold-changes of >1.2 as significant. In addition, Gene Ontology (GO) was used to describe molecular functions, cellular components and biological processes. Kyoto Encyclopedia of Genes and Genomes (KEGG) pathway was used to draw pathway maps representing our knowledge of the molecular interaction and reaction networks.

Western blot analysis. The conditioned media of CNE-2 and CNE-2R cells with protease inhibitor tablets (Roche Applied Science, Mannheim, Germany) were concentrated to an approximate volume of 300 μl using 3 kDa cut-off Amicon Ultra-15 centrifugal filters (Millipore, Bedford, MA, USA) at 5,000 x g and 4˚C. CNE-2 and CNE-2R cells were lysed with radioimmunoprecipitation assay (RIPA) lysis buffer (Beyotime Institute of Biotechnology, China) for 30 min and then centrifuged at 12,000 x g at 4˚C for 20 min, to obtain the cell extracts. Equal amounts of protein were separated by sodium dodecyl sulfate-polyacrylamide gel electrophoresis (for fibrillin-2, 6%; for CD166 and sulfhydryl oxidase 1, 10%; for cofilin-2, 15%) before transfer onto polyvinylidene fluoride membranes (Millipore). The membranes were blocked with 5% non-fat dried milk for 1 h at room temperature with gentle shaking. Immunodetection was performed by incubating at 4˚C with antibodies against fibrillin-2 (diluted 1:150; Santa Cruz Biotechnology, Santa Cruz, CA, USA), CD166 (diluted 1:1,500), sulfhydryl oxidase 1 (diluted 1:1,000), cofilin-2 (diluted 1:1,000) (all from Abcam, Cambridge, MA, USA), and glyceraldehyde-3-phosphate dehydrogenase (GAPDH) (diluted 1:5,000; ProteinTech Group, Chicago IL, USA) as a loading control. After washing and incubating with fluorescently labeled goat anti-mouse/rabbit IgG secondary antibody (diluted 1:15,000; Cell Signaling Technology, Inc., Beverly, MA, USA), the fluorescence intensity was detected using an Odyssey Infrared Imaging System (Odyssey version 3.0.X; LI-COR Biosciences, Lincoln, NE, USA).

Immunocytochemistry. In each well of a 24-well plate, 3,000 cells were inoculated at 37˚C. When cell fusion reached

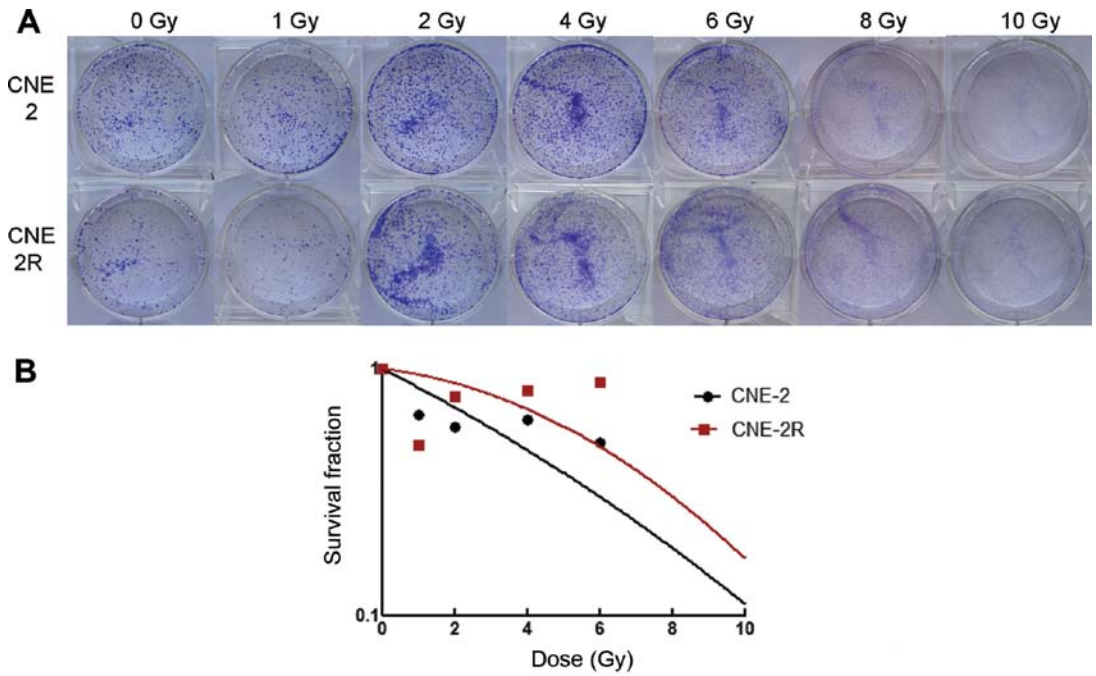

Figure 1. Colony formation assays for radiosensitivity. (A) Colony formation assays of the CNE-2 and CNE-2R cell lines were performed to evaluate radiosensitivity. (B) The fit curves were analyzed using GraphPad Prism 5.0 software.

60-70%, the cells were washed 3 times with 2 ml PBS and fixed for 20 min in 4% paraformaldehyde at room temperature, followed by 3 more washes with PBS. The cells were then blocked for endogenous peroxidase activity with 3% H_2O_2 for 15 min at room temperature, followed by 3 washes with PBS and blocked for 20 min with 5% BSA in PBS. The cells were incubated with anti-CD166 primary antibodies (diluted 1:100; Abcam) at 4˚C overnight. PBS was used for negative controls. After washing 3 times, the cells were then incubated with biotin-labeled goat anti-rabbit antibody for 12 min at room temperature and subsequently incubated with streptavidin-conjugated horseradish peroxidase (HRP) (both from Zhongshan Inc., Zhongshan, China) for 12 min. Cells were treated with diaminobenzidine (DAB) (Zhongshan Inc.) for 4 min and counterstained with hematoxylin for 20 sec. Images were captured under a phase-contrast microscope (IX71).

Statistical analysis. Data are expressed as means ± standard deviations. Comparisons of parameters between the two groups were performed with the Student's t-test using SPSS 16.0 (SPSS, Inc., Chicago, IL, USA). A value of $p<0.05$ was considered to indicate a statistically significant result.

Results

Radiation sensitivity of the CNE-2 and CNE-2R cell lines. We observed the survival curves of the CNE-2 and CNE-2R cell lines by colony formation assays. The radiation dose-responses of the different cells are shown in Fig. 1A. There were fewer surviving colonies of CNE-2R cells than CNE-2 at doses of 0 or 1 Gy, while there were more surviving CNE-2R colonies than CNE-2 colonies at doses of 2-10 Gy. GraphPad Prism 5.0 software was used to analyze the fit curves shown in Fig. 1B. The CNE-2R survival curves were significantly higher than the survival curves for CNE-2. The radiobiology parameters are shown in Table I. Parameters α and α/β of the CNE-2 cells were higher than these parameters for the CNE-2R cells (α, p=0.003; α/β, p=0.010), where α is regarded as a parameter that reflects the intrinsic radiosensitivity. and α/β measures cell repair capacity (25). The higher value of α and higher ratio of α/β indicated that the repair capacity was weaker. Parameter β of CNE-2 was lower than that for CNE-2R (p=0.04), where β is interpreted as a reflection of the repair of sublethal DNA damage induced by the first dose. The lower value of β indicated that the recovery capacity was weaker. Thus, we suggested that the repair capability of the CNE-2R cells was stronger than that for CNE-2. All the above suggest that CNE-2R cells are radioresistant.

Table I. Radiobiology parameters (the linear-quadratic model).

Cell line	α	β	α/β
CNE-2	0.1634±0.0351	0.0063±0.0010	26.9240±9.4105
CNE-2R	0.0258±0.01183	0.0174±0.0030	1.5867±0.9937
P-value	0.003	0.004	0.010

Cell viability. Cell viability was determined using trypan blue dye and cell counting under a phase-contrast microscope. Dead cells were defined as cells that were stained with the dye and turned blue. The percentage of living cells was calculated by the relationship between the number of viable cells and the total number of cells counted. As shown in Fig. 2A, ~1 cell in 100 was stained with the dye, and the cells preserved good viability when kept for ~24 h in conditioned media without serum. The diagrams shown in Fig. 2B represent the percentages of viable

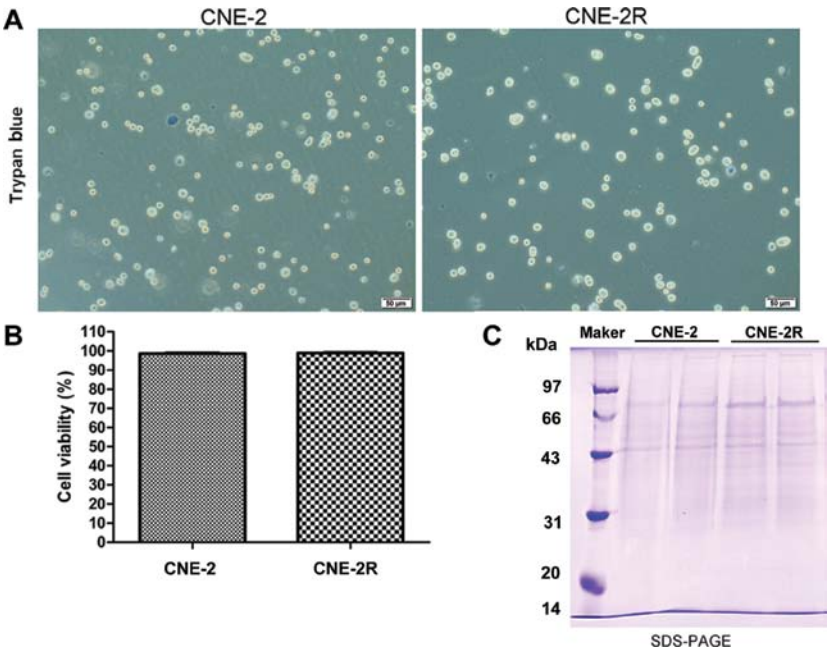

Figure 2. Trypan blue dye exclusion assays and cell counting were used to determine viable cell numbers, and SDS-PAGE assays were used to analyze the conditioned media harvested from the CNE-2 and CNE-2R cells. (A) The conditioned media and adherent cells of CNE-2 and CNE-2R were dyed to exclude dead cells using trypan blue dye. The cells that turned blue were considered dead cells (magnification, x100). (B) The conditioned media and adherent cells of CNE-2 and CNE-2R were used to determine viable cell numbers. (C) The conditioned media of CNE-2 and CNE-2R cells were precipitated and processed as described in Materials and methods. Proteins (5 μg) were resolved on 10% SDS gel and stained with Coomassie blue.

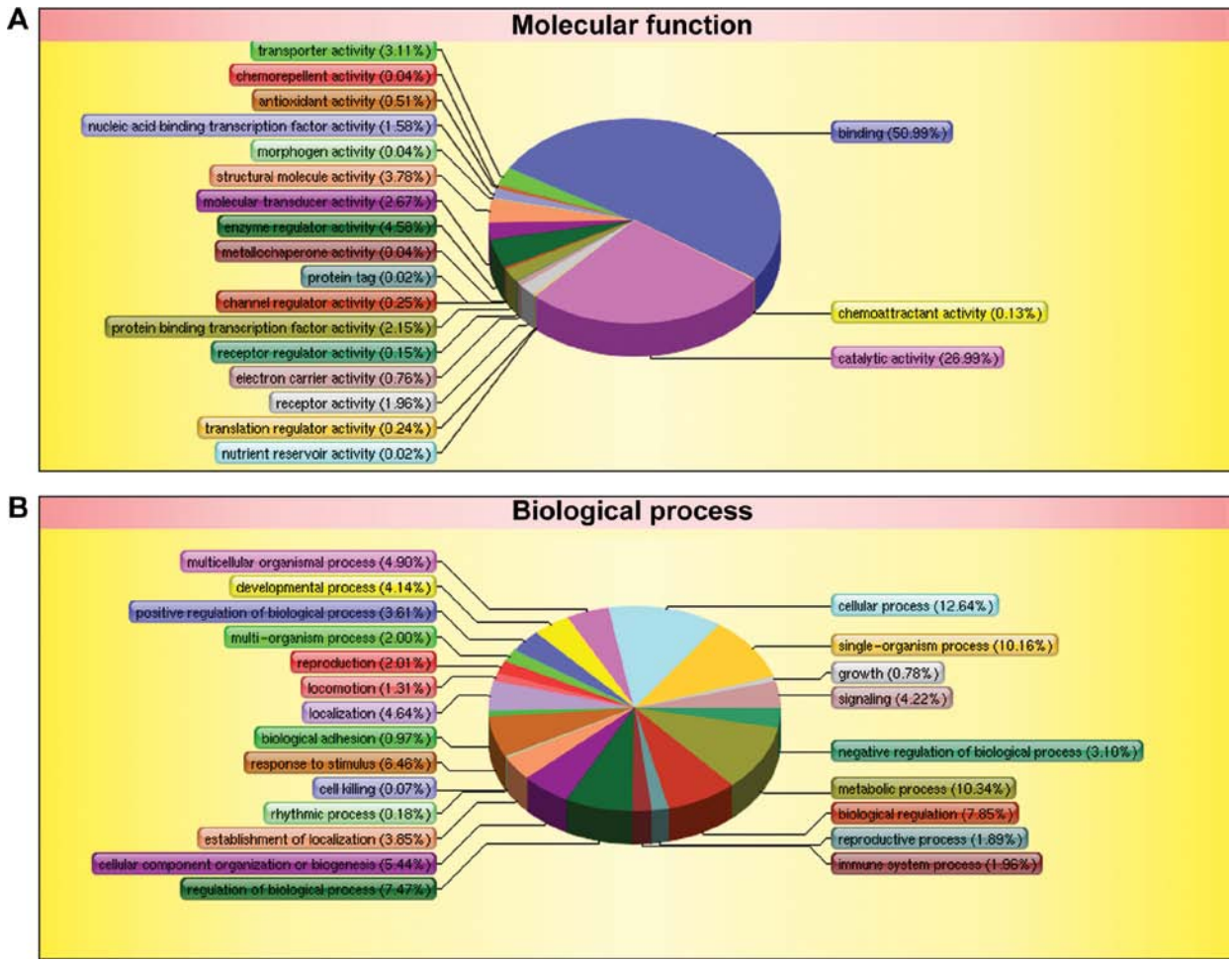

Figure 3. Identification of secretory proteins in the CNE-2 and CNE-2R cell lines. (A) Molecular functional classification of the 3,581 total identified proteins. The pie chart shows the distribution of identified proteins into their functional classes by percentage. (B) Biological processes of the 3,581 total identified proteins. The pie chart shows the distribution of identified proteins into their biological process classes by percentage.

Table II. Differentially secreted proteins in the CNE-2 and CNE-2R cells.

No.	Accession (tr, sp)	Protein name	Score	Fold-change CNE-2/CNE-2R	Fold-change CNE-2/CNE-2R(1)	Fold-change CNE-2/CNE-2R(2)	Signal peptide	Secretory protein
1	tr|D6RJI3|D6RJI3_HUMAN	Fibrillin-2	6,984	1.466	1.421	1.551	Yes	Yes
2	sp|O00391|QSOX1_HUMAN	Sulfhydryl oxidase 1	4,872	1.494	1.322	1.785	Yes	Yes
3	sp|P12109|CO6A1_HUMAN	Collagen α-1 (VI) chain	1,613	0.777	0.696	0.862	Yes	Yes
4	sp|P30043|BLVRB_HUMAN	Flavin reductase (NADPH)	880	0.834	0.658	0.854	No	Yes
5	sp|Q9Y281-3|COF2_HUMAN	Isoform 3 of cofilin-2	701	0.516	0.44	0.599	No	Yes
6	sp|Q13740-2|CD166_HUMAN	Isoform 2 of CD166 antigen	671	0.597	0.585	0.788	Yes	Yes
7	sp|Q9HB07|MYG1_HUMAN	UPF0160 protein MYG1, mitochondrial	642	0.855	0.834	0.819	Yes	Yes
8	tr|Q6MZW0|Q6MZW0_HUMAN	Putative uncharacterized protein DKFZp686J11235	611	2.217	2.474	1.745	Yes	Yes
9	sp|P62857|RS28_HUMAN	40S ribosomal protein S28 HCG26477	577	0.613	0.775	0.524	No	Yes
10	sp|Q86SQ4-2|GP126_HUMAN	Isoform 2 of G-protein coupled receptor 126	555	1.222	1.123	1.385	Yes	Yes
11	tr|D3DR24|D3DR24_HUMAN	Exostoses (multiple) 2, isoform CRA_a	470	1.317	1.231	1.461	No	Yes
12	tr|A8K878|A8K878_HUMAN	cDNA FLJ77177	401	0.586	0.625	0.583	Yes	Yes
13	tr|F5H1G4|F5H1G4_HUMAN	Neuropilin-2	392	2.226	2.326	1.848	Yes	Yes
14	tr|Q5HYL6|Q5HYL6_HUMAN	Putative uncharacterized protein DKFZp686E1899	341	0.805	0.842	0.746	No	Yes
15	tr|B4DJS7|B4DJS7_HUMAN	Sorting nexin 6, isoform CRA_e	222	0.787	0.786	0.753	Yes	Yes
16	sp|Q13219|PAPP1_HUMAN	Pappalysin-1	216	1.817	1.727	1.667	Yes	Yes
17	tr|Q5JNW7|Q5JNW7_HUMAN	Proteasome subunit β type-8	205	0.554	0.643	0.583	No	Yes
18	sp|P10606|COX5B_HUMAN	Cytochrome *c* oxidase subunit 5B, mitochondrial	201	0.687	0.734	0.645	No	Yes

tr, tremble; sp, swissprot.

cells in the CNE-2 and CNE-2R cell lines. Both CNE-2 and CNE-2R cells kept in serum-free conditioned media for 24 h exhibited >99% cell viability. We focused on studying the secretory proteins and excluded the proteins from dead cells that polluted the conditioned media, as feasible.

Proteins extracted from conditioned media of the CNE-2 and CNE-2R cells show repeatability. Due to the heterogeneity of protein samples and the wide range of protein contents from each precipitation, we used SDS-PAGE to ensure the material precipitated from conditioned media using acetone was really 'protein' and to confirm the repeatability of the samples. CNE-2 and CNE-2R cells were cultured in serum-free medium for 24 h, and then the culture supernatants were collected. After concentration, the proteins were resolved on 10% SDS gels and stained with Coomassie blue (Fig. 2C). The protein-staining pattern of conditioned media was shown to demonstrate that the secreted proteins were enriched in the culture media. The bands were similar between CNE-2 duplicates and between CNE-2R and duplicates, demonstrating repeatability. In addition, the bands were different between the CNE-2 and CNE-2R cells, indicating that the secretory proteins were differentially enriched in CNE-2 and its radioresistant cell line CNE-2R.

Prediction of secretory proteins that were differentially expressed in the CNE-2 and CNE-2R cells. Proteins that were preliminarily identified as being differentially expressed in NPC cells were identified by iTRAQ labeling followed by LC-ESI-MS/MS analysis and searching with the Mascot search engine. The 3,581 identified proteins were functionally classified on the basis of universal GO annotation terms and were linked to at least one annotation term each within the GO molecular function and biological process categories. As shown in Fig. 3A, the top three molecular functions were protein binding (50.99%), catalytic activity (26.99%) and enzyme regulator activity (4.50%). In Fig. 3B, the top three biological process categories were cellular processes (12.64%), metabolic processes (10.34%) and single-organism processes (10.16%). Among the 3,581 proteins, 40 were associated with significant database hits. Among these 40 significant differentially expressed proteins in the CNE-2 and CNE-2R cells, 11 proteins were predicted by SignalP 3.0 (http://www.cbs.dtu.dk/services/SignalP-3.0/) to be secreted in the classical secretory pathway (14,26), which is characterized by the presence of a signal peptide. Seven proteins were predicted by Secretome 2.0 (http://www.cbs.dtu.dk/services/SecretomeP/) to be released through the non-classical secretory pathway (27,28) (Supporting Information Table II), which is characterized by non-classically secreted proteins that obtain an NN-score exceeding the normal threshold of 0.5 but are not predicted to contain a signal peptide. However, 22 proteins remained unconfirmed. Exosomal release is also a form of nonclassical secretion mechanism. Potential exosomal release of the proteins was studied by manual annotation of the ExoCarta exosome database (http://exocarta.ludwig.edu.au/) (27,29,30). Eight proteins were predicted by the ExoCarta exosome database to be secreted in the exosomal pathway (Supporting Information Table III). Altogether, the profile analyses predicted that 65% [(11+7+8)/40] of the identified

Table III. Significant difference in secretory proteins between CNE-2 and CNE-2R cells were predicted by ExoCarta exosome database.

No.	Accession (tr, sp)	Protein name	Score	Fold-change CNE-2/CNE-2R	Fold-change CNE-2-119 vs. CNE-2R-113	Fold-change CNE-2-121 vs. CNE-2R-115	Secretory protein
1	sp|P13647|K2C5_HUMAN	Keratin, type II cytoskeletal 5	3,881	2.259	1.568	3.730	Yes
2	tr|G3V1V0|G3V1V0_HUMAN	Myosin light polypeptide 6	985	0.698	0.786	0.700	Yes
3	sp|Q96QK1|VPS35_HUMAN	Vacuolar sorting-associated protein 35	877	1.268	1.280	1.401	Yes
4	sp|P80723|BASP1_HUMAN	Brain acid soluble protein 1	504	0.722	0.789	0.689	Yes
5	tr|B1AHD1|B1AHD1_HUMAN	NHP2-like protein 1	305	0.701	0.829	0.580	Yes
6	tr|Q6FH57|Q6FH57_HUMAN	Peptidyl-prolyl *cis*-trans isomerase	262	0.557	0.543	0.551	Yes
7	sp|P10606|COX5B_HUMAN	Cytochrome *c* oxidase subunit 5B	201	0.687	0.734	0.645	Yes
8	sp|Q4G0F5|VP26B_HUMAN	Vacuolar sorting-associated 26B	187	0.749	0.610	0.794	Yes

tr, tremble; sp, swissprot.

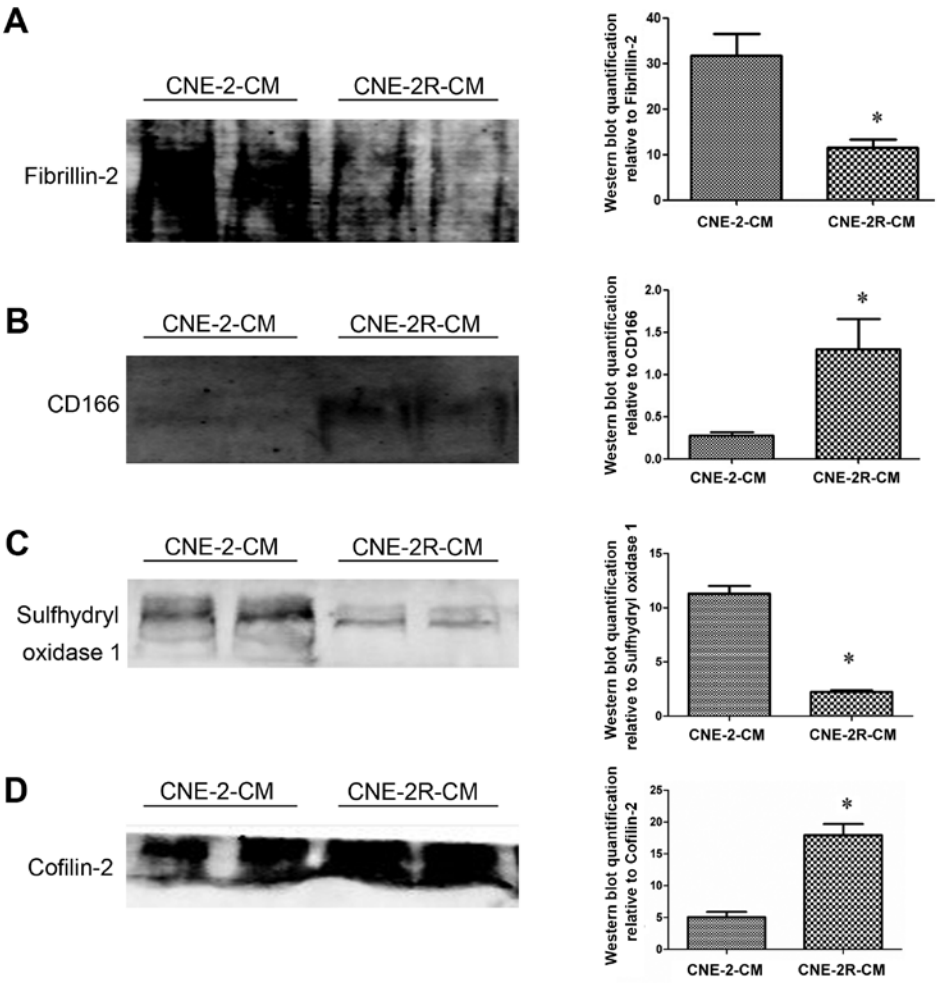

Figure 4. Confirmation of the results of the proteomics by western blotting. Conditioned media (CM) were resolved on SDS-PAGE gels, transferred onto PVDF membranes, and probed with specific antibodies against the indicated targets. The histograms to the right of the blots represent the relative quantification levels as determined by the Odyssey Infrared Imaging System. (A) The secretory protein fibrillin-2 at 350 kDa was confirmed. *p=0.017 vs. CNE-2-CM. (B) The secretory protein of CD166 at 105 kDa was confirmed. *p=0.012 vs. CNE-2-CM. (C) The secretory protein sulfhydryl oxidase 1 (known as Quiescin Q6) at 83 kDa was confirmed. *p=0.000 vs. CNE-2-CM. (D) The secretory protein cofillin-2 at 18 kDa was confirmed. *p=0.003 vs. CNE-2-CM.

proteins could be released into conditioned media and related to radioresistance in NPC cells.

Validation of the differential expression of the secretory proteins by western blotting. To confirm the expression levels of the differentially expressed proteins identified by a proteomic approach, the expression of four differentially expressed secretory proteins (fibrillin-2, CD166, sulfhydryl oxidase 1, cofilin-2) in the conditioned media of CNE-2 and CNE-2R cells were detected by western blotting. As shown in Fig. 4, fibrillin-2 and sulfhydryl oxidase 1 were downregulated in CNE-2R compared with levels in the CNE-2 cells, whereas CD166 and cofilin-2 were upregulated in the CNE-2R cells compared with levels in the CNE-2 cells. As shown in Fig. 4, the columns showed that the protein levels of four secretory proteins were significantly different in conditioned media between the CNE-2 and CNE-2R cells (fibrillin-2, p=0.017; sulfhydryl oxidase 1, p=0.000; CD166, p=0.012; cofilin-2, p=0.003), which was consistent with the proteomic prediction results. In addition, we compared the four proteins in the cell extracts of the CNE-2 and CNE-2R cells. As shown in Fig. 5, the secretory proteins fibrillin-2 and sulfhydryl oxidase 1 were not expressed in the NPC cells, whereas CD166 was down-regulated in the CNE-2R cells when compared with that in the CNE-2 cells (p=0.001) and cofilin-2 was upregulated in the CNE-2R compared with that in the CNE-2 cells (p=0.003).

CD166 protein was expressed in the CNE-2 and CNE-2R cells. To investigate the expression of CD166 protein in the CNE-2 and CNE-2R cells, immunocytochemical detection was performed. Representative staining patterns for CD166 are shown in Fig. 6. CD166 protein expression, shown by brown-yellow staining, was observed in both the CNE-2 and CNE-2R cells. CD166 was only expressed in a few cells. In the negative control group, the cells were not stained. These results showed that CD166 was expressed in the CNE-2 and CNE-2R cells of NPC.

Discussion

Radioresistance remains a major issue in the treatment of nasopharyngeal carcinoma (NPC) (31), and the molecular mechanisms underlying NPC radioresistance remain unclear. To date, there have been no effective serum biomarkers for

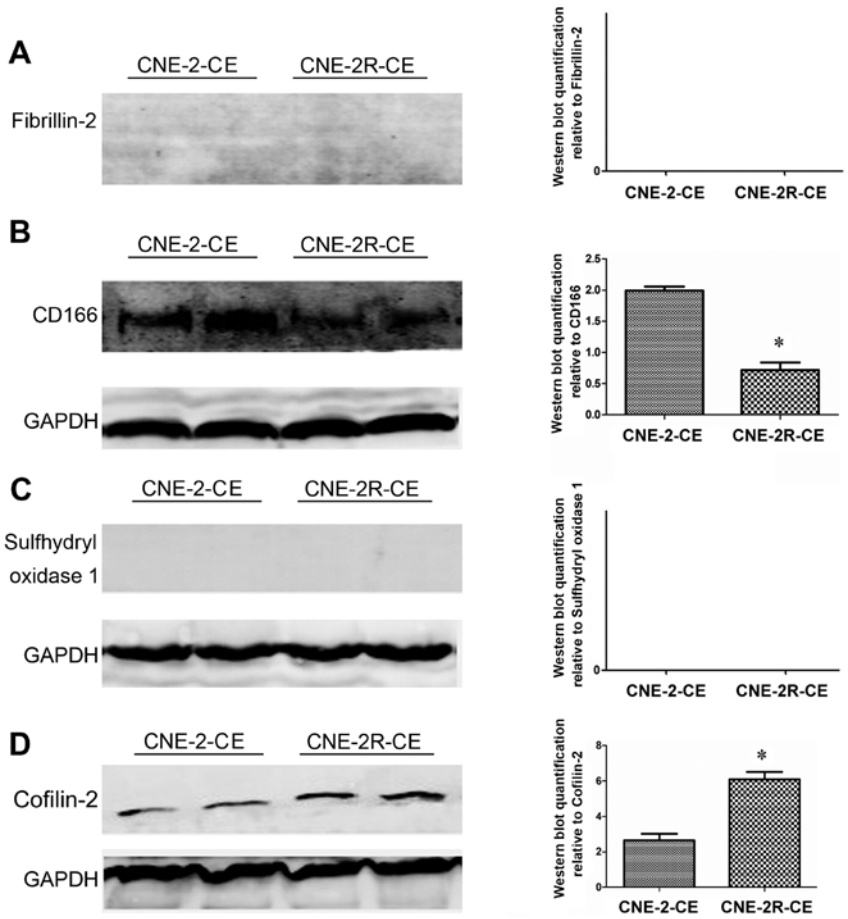

Figure 5. The differential expression of four proteins between CNE-2 and CNE-2R in the cell extract (CE). GAPDH was used as a loading control. The histograms to the right of the blots represent relative quantification levels as determined by the Odyssey Infrared Imaging System. (A) The secretory protein fibrillin-2 at 350 kDa was confirmed. Due to its high molecular weight, it lacked an appropriate loading control. (B) The secretory protein CD166 at 105 kDa was confirmed. *p<0.05 vs. CNE-2-CE. (C) The secretory protein sulfhydryl oxidase 1 (known as Quiescin Q6) at 83 kDa was confirmed. (D) The secretory protein cofillin-2 at 18 kDa was confirmed. *p<0.05 vs. CNE-2-CE.

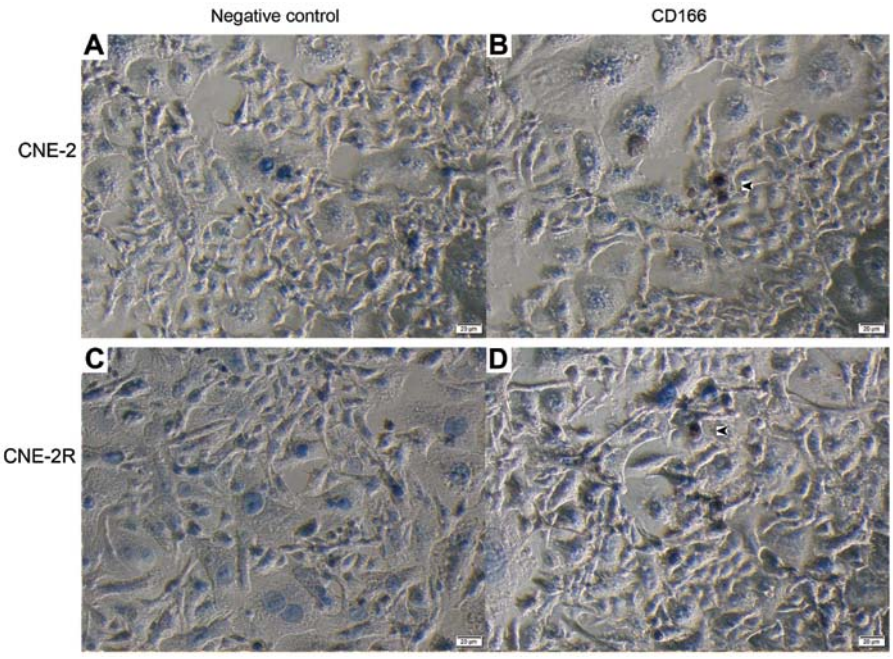

Figure 6. Immunocytochemical detection of CD166 expression in the CNE-2 and CNE-2R cells (magnification, x200). Cells were counterstained with hematoxylin, and nuclei are indicated by blue staining. CD166 protein expression is shown by brown-yellow staining and indicated by arrows. (A and C) Negative control (PBS without antibody was used) did not express CD166 in the CNE-2 and CNE-2R cells. (B and D) As indicated by the arrows, the experimental group expressed CD166 in the CNE-2 and CNE-2R cells.

Table IV. Pathways involving cofilin-2 or CD166 were predicted by KEGG pathway.

No.	Pathways	Proteins (tr, sp)
1	Regulation of actin cytoskeleton (no map in KEGG database)	sp|O14974-3|MYPT1_HUMAN, **sp|Q9Y281-3|COF2_HUMAN**, sp|Q9Y2A7-2|NCKP1_HUMAN, etc.
2	Axon guidance (no map in KEGG database)	sp|O15031|PLXB2_HUMAN, **sp|Q9Y281-3|COF2_HUMAN**, tr|A0PK02|A0PK02_HUMAN, etc.
3	Fcγ R-mediated phagocytosis (no map in KEGG database)	sp|O15143|ARC1B_HUMAN, **sp|Q9Y281-3|COF2_HUMAN,** sp|Q9Y6W5|WASF2_HUMAN, etc.
4	Pertussis (no map in KEGG database)	sp|O75973|C1QRF_HUMAN, **sp|Q9Y281-3|COF2_HUMAN**, sp|Q9Y4K3|TRAF6_HUMAN, etc.
5	Cell adhesion molecules (CAMs) (no map in KEGG database)	sp|O75131|CPNE3_HUMAN, **sp|Q13740-2|CD166_HUMAN,** sp|Q68D85|NR3L1_HUMAN, etc.

tr, tremble; sp, swissprot. KEGG, Kyoto Encyclopedia of Genes and Genomes.

predicting NPC radiosensitivity. The identification of NPC radioresistance-associated secretory proteins will help to find biomarkers to estimate NPC response to radiotherapy and reveal the molecular mechanisms of NPC radioresistance.

In the present study, we used acetone to precipitate conditioned media and applied the iTRAQ labeling proteomic approach to screen different secretory proteins between CNE-2R and its parental CNE-2 cells. Before quantitative proteomic analysis, we investigated the survival curves of the CNE-2 and CNE-2R cell lines by colony formation assays, and the CNE-2R survival curves were significantly higher than the CNE-2 curves (Fig. 1). Afterwards, a trypan blue dye exclusion assay was performed to exclude the dead cells that could pollute the conditioned media of secretory proteins (Fig. 2). A total of 40 significantly different proteins were identified, of which 26 were predicted to be secretory proteins by SignalP 3.0, Secretome 2.0 and ExoCarta exosome database (Tables II and III). Four (fibrillin-2, 350 kDa; CD166, 105 kDa; sulfhydryl oxidase 1, 83 kDa; cofilin-2, 18 kDa) of these 26 secretory proteins were also quantified by western blotting and the results were consistent with the results of the iTRAQ labeling proteomic approach (Fig. 4). This result suggested that the proteins identified by the iTRAQ labeling proteomic approach were actually differentially expressed proteins. In addition, the expression of the four proteins in NPC cells was detected by western blotting, as shown in Fig. 5. According to the western blotting bands and columns, fibrillin-2 and sulfhydryl oxidase 1 were not expressed in the NPC cells (CNE-2 and CNE-2R), while cofilin-2 and CD166 were expressed in the NPC cells. Finally, immunocytochemistry was performed to further examine the expression of CD166 in the radiosensitive CNE-2 and radioresistant CNE-2R cells, and the images of their expression were observed.

Fibrillin-2 is a molecule that contributes to the structural integrity of the extracellular matrix. Recently, data relating to the expression of fibrillin-2 in human cancers were reported. For example, fibrillins interact with integrins and heparin-sulfated proteoglycans and most likely play important roles in cell migration, adhesion, signaling and differentiation. They are important in the processes of tumor growth and metastasis (32). Fibrillin-2 transcript and protein are also densely present in rhabdomyosarcoma (33). Various studies have revealed that the LTBP/fibrillin family form integral components of the fibronectin and microfibrillar extracellular matrix (ECM), are related to breast cancers, and may promote metastasis by providing the bridge between structural and signaling components of the epithelial to mesenchymal transition (34). However, in the present study, the level of secretory protein fibrillin-2 was far lower in CNE-2R than that in the CNE-2 cells. The reasons may be as follows: CNE-2R was generated from CNE-2 by radiation. Radiation could trigger the endoplasmic reticulum (ER) to activate a survival pathway in cancer cells (35). ER stress triggers may induce cellular removal through the unfolded protein response pathway (36). Fibrillin-2 forms large fibrillar structures within the rough endoplasmic reticulum (rER) in association with an unfolded protein response (37). We presumed that radiation induced an increase in the unfolded protein response pathway and led to decreased expression of the fibrillin-2-mediated unfolded protein response pathway. As a result, fibrillin-2 was expressed less in the CNE-2R than that in CNE-2 cells.

Sulfhydryl oxidase 1, also known as Quiescin Q6, catalyzes the oxidation of sulfhydryl groups in peptide and protein thiols to disulfides with the reduction of oxygen to hydrogen peroxide. It may contribute to disulfide bond formation in a variety of secreted proteins. In fibroblasts, it may have tumor-suppressing capabilities involved in growth regulation (38-40). It is not difficult to explain why the expression of sulfhydryl oxidase 1 was lower in CNE-2R than in CNE-2 cells, as shown in Fig. 4C. CNE-2R is a radioresistant cell line, and its

tumor-suppressing capabilities are naturally lower than that of CNE-2 cells.

Cofilin-2 reversibly controls actin polymerization and depolymerization in a pH-sensitive manner. Some studies have reported cofilins to be important regulators of the actin cytoskeleton, whose upregulation of the actin cytoskeleton enhances tumor cell migration and invasion (41) and to regulate cell protrusion and motility through the spatial interaction of the lamellipodium and lamella (42). Cofilin-2 exhibits significantly lower expression in pancreatic cancerous tissues compared to non-cancerous tissues (43). Recently, malignant progressive tumor cell clones have also been reported to exhibit significant upregulation of cofilin-2 compared to regressive clones (44). In the present study, cofilin-2 was highly expressed in the CNE-2R cells compared to that in the CNE-2 cells (Figs. 4 and 5). Table IV shows that cofilin-2 is involved in the pathways of regulation of the actin cytoskeleton (41), axon guidance (45) and Fcγ R-mediated phagocytosis (46) related to the migration, invasion and development of tumor cells, as predicted by KEGG pathway. This may imply that the more cofilin-2 is expressed, the more cells migrate and invade. However, we should also consider the opinion that starvation-induced autophagy is a mechanism that promotes cell survival, and it has yet to be revealed whether starvation-induced cell autophagy is related to cofilin-2 expression (47). In the present study, before the proteomic assay, CNE-2 and CNE-2R cells were cultured by serum-free conditioned media starvation for 24 h. Thus, cofilin-2 may be related to the struggle between cancerous and non-cancerous tissue under conditions of starvation. Whether cofilin-2 is involved in starvation resistance by a self-regulating protective mechanism in normal tissue cells during the migration and invasion of NPC cells must be clarified by further study.

CD166 is also known as activated leukocyte cell adhesion molecule (ALCAM)/MEMD and has been identified as a positive marker of mesenchymal stem cells (MSCs) (48-50), which have a close relationship with cancer stem cells (CSCs) (51) and as a positive marker of CSCs (52,53). Yan *et al* (54) found that relative to CD166(low) head and neck squamous cell carcinoma (HNSCC) cells, CD166(high) HNSCC cells exhibited greater sphere-formation ability *in vitro* and tumor formation ability. However, the 'cancer stem cell' (CSC) theory was first stated by Nowell in 1978 (55) which supported the idea that human cancer can be considered as a stem cell disease which was proposed in 2001 (56). According to the CSC theory, only a phenotypic subset of cancer cells within each tumor is capable of initiating tumor growth. In the present study, as shown in Fig. 6, a phenotypic subset of CD166-positive cells was applied to immunocytochemistry of NPC cells. To our surprise, CD166 was expressed in a few NPC cells. It was inferred that CSCs may exist in NPC cells and that CD166 may be a positive marker of CSCs in NPC. In addition, as shown in Table IV, CD166 is involved in the pathway of cell adhesion molecules related to the proliferation of tumor cells, as predicted by KEGG pathway. Overall, CD166 plays an important role in NPC.

In summary, we used the iTRAQ labeling proteomic approach to identify differential secretory proteins between the radioresistant CNE-2R and its parental CNE-2 cell line, and 26 secretory proteins were identified. We showed that the abnormal expression of fibrillin-2, CD166, sulfhydryl oxidase 1 and cofilin-2 according to western blot analyses may serve as potential biomarkers for predicting NPC response to radiotherapy. Amazingly, we showed that the positive cancer stem cell marker CD166 was positive in NPC cells. This result calls for further investigation, such as sorting the cancer stem cells from NPC patients by fluorescence-activated cell sorting (FACS) or magnetic-activated cell sorting (MACS), spheroid colony formation assays and a nude mouse model. Cancer stem cells possess the ability to sustain tumor self-renewal, which may contribute to the radioresistance in NPC.

Acknowledgements

The present study was supported by grants from the Natural Science Foundation of China (81360343), the Key Laboratory of Guangxi Special Fund (GK2013-13-A-02-01) and the Key Research of Guangxi Medical Hygiene Program (zhong2011076).

References

1. He ML, Luo MX, Lin MC and Kung HF: MicroRNAs: Potential diagnostic markers and therapeutic targets for EBV-associated nasopharyngeal carcinoma. Biochim Biophys Acta 1825: 1-10, 2012.
2. Lo KW, To KF and Huang DP: Focus on nasopharyngeal carcinoma. Cancer Cell 5: 423-428, 2004.
3. Chia WK, Teo M, Wang WW, Lee B, Ang SF, Tai WM, Chee CL, Ng J, Kan R, Lim WT, *et al*: Adoptive T-cell transfer and chemotherapy in the first-line treatment of metastatic and/or locally recurrent nasopharyngeal carcinoma. Mol Ther 22: 132-139, 2014.
4. Wu J, Tang Q, Zhao S, Zheng F, Wu Y, Tang G and Hahn SS: Extracellular signal-regulated kinase signaling-mediated induction and interaction of FOXO3a and p53 contribute to the inhibition of nasopharyngeal carcinoma cell growth by curcumin. Int J Oncol 45: 95-103, 2014.
5. Suárez C, Rodrigo JP, Rinaldo A, Langendijk JA, Shaha AR and Ferlito A: Current treatment options for recurrent nasopharyngeal cancer. Eur Arch Otorhinolaryngol 267: 1811-1824, 2010.
6. Lee AW, Ng WT, Chan LL, Hung WM, Chan CC, Sze HC, Chan OS, Chang AT and Yeung RM: Evolution of treatment for nasopharyngeal cancer - success and setback in the intensity-modulated radiotherapy era. Radiother Oncol 110: 377-384, 2014.
7. Good DM, Thongboonkerd V, Novak J, Bascands JL, Schanstra JP, Coon JJ, Dominiczak A and Mischak H: Body fluid proteomics for biomarker discovery: Lessons from the past hold the key to success in the future. J Proteome Res 6: 4549-4555, 2007.
8. Schmidt A and Aebersold R: High-accuracy proteome maps of human body fluids. Genome Biol 7: 242, 2006.
9. Reymond MA and Schlegel W: Proteomics in cancer. Adv Clin Chem 44: 103-142, 2007.
10. Hanash SM, Pitteri SJ and Faca VM: Mining the plasma proteome for cancer biomarkers. Nature 452: 571-579, 2008.
11. Juan HF, Chen JH, Hsu WT, Huang SC, Chen ST, Yi-Chung Lin J, Chang YW, Chiang CY, Wen LL, Chan DC, *et al*: Identification of tumor-associated plasma biomarkers using proteomic techniques: From mouse to human. Proteomics 4: 2766-2775, 2004.
12. Wu CC, Chien KY, Tsang NM, Chang KP, Hao SP, Tsao CH, Chang YS and Yu JS: Cancer cell-secreted proteomes as a basis for searching potential tumor markers: Nasopharyngeal carcinoma as a model. Proteomics 5: 3173-3182, 2005.
13. Wu CC, Peng PH, Chang YT, Huang YS, Chang KP, Hao SP, Tsang NM, Yeh CT, Chang YS and Yu JS: Identification of potential serum markers for nasopharyngeal carcinoma from a xenografted mouse model using Cy-dye labeling combined with three-dimensional fractionation. Proteomics 8: 3605-3620, 2008.
14. Chang KP, Wu CC, Chen HC, Chen SJ, Peng PH, Tsang NM, Lee LY, Liu SC, Liang Y, Lee YS, *et al*: Identification of candidate nasopharyngeal carcinoma serum biomarkers by cancer cell secretome and tissue transcriptome analysis: Potential usage of cystatin A for predicting nodal stage and poor prognosis. Proteomics 10: 2644-2660, 2010.

15. Tang S, Huang W, Zhong M, Yin L, Jiang H, Hou S, Gan P and Yuan Y: Identification Keratin 1 as a cDDP-resistant protein in nasopharyngeal carcinoma cell lines. J Proteomics 75: 2352-2360, 2012.
16. Gu SY, Tang WP, Zeng Y, *et al*: An epithelial cell line established from poorly differentiated nasopharyngeal carcinoma. Ai Zheng 2: 70-72, 1983 (In Chinese).
17. Li GP, Wang H, Lai YK, Chen SC, Lin MC, Lu G, Zhang JF, He XG, Qian CN and Kung HF: Proteomic profiling between CNE-2 and its strongly metastatic subclone S-18 and functional characterization of HSP27 in metastasis of nasopharyngeal carcinoma. Proteomics 11: 2911-2920, 2011.
18. Guo Y, Zhu XD, Qu S, Li L, Su F, Li Y, Huang ST and Li DR: Identification of genes involved in radioresistance of nasopharyngeal carcinoma by integrating gene ontology and protein-protein interaction networks. Int J Oncol 40: 85-92, 2012.
19. Petriz BA, Gomes CP, Rocha LA, Rezende TM and Franco OL: Proteomics applied to exercise physiology: A cutting-edge technology. J Cell Physiol 227: 885-898, 2012.
20. Jayapal KP, Sui S, Philp RJ, Kok YJ, Yap MG, Griffin TJ and Hu WS: Multitagging proteomic strategy to estimate protein turnover rates in dynamic systems. J Proteome Res 9: 2087-2097, 2010.
21. Zhou ZR, Zhu XD, Zhao W, Qu S, Su F, Huang ST, Ma JL and Li XY: Poly(ADP-ribose) polymerase-1 regulates the mechanism of irradiation-induced CNE-2 human nasopharyngeal carcinoma cell autophagy and inhibition of autophagy contributes to the radiation sensitization of CNE-2 cells. Oncol Rep 29: 2498-2506, 2013.
22. Tang CE, Guan YJ, Yi B, Li XH, Liang K, Zou HY, Yi H, Li MY, Zhang PF, Li C, *et al*: Identification of the amyloid β-protein precursor and cystatin C as novel epidermal growth factor receptor regulated secretory proteins in nasopharyngeal carcinoma by proteomics. J Proteome Res 9: 6101-6111, 2010.
23. Li S, Li X, Wang Y, Yang J, Chen Z and Shan S: Global secretome characterization of A549 human alveolar epithelial carcinoma cells during *Mycoplasma pneumoniae* infection. BMC Microbiol 14: 27, 2014.
24. Lyu SY, Rhim JY and Park WB: Antiherpetic activities of flavonoids against herpes simplex virus type 1 (HSV-1) and type 2 (HSV-2) in vitro. Arch Pharm Res 28: 1293-1301, 2005.
25. van den Aardweg GJ, Kiliç E, de Klein A and Luyten GP: Dose fractionation effects in primary and metastatic human uveal melanoma cell lines. Invest Ophthalmol Vis Sci 44: 4660-4664, 2003.
26. Bendtsen JD, Nielsen H, von Heijne G and Brunak S: Improved prediction of signal peptides: SignalP 3.0. J Mol Biol 340: 783-795, 2004.
27. Loei H, Tan HT, Lim TK, Lim KH, So JB, Yeoh KG and Chung MC: Mining the gastric cancer secretome: Identification of GRN as a potential diagnostic marker for early gastric cancer. J Proteome Res 11: 1759-1772, 2012.
28. Bendtsen JD, Jensen LJ, Blom N, Von Heijne G and Brunak S: Feature-based prediction of non-classical and leaderless protein secretion. Protein Eng Des Sel 17: 349-356, 2004.
29. Nickel W: The mystery of nonclassical protein secretion. A current view on cargo proteins and potential export routes. Eur J Biochem 270: 2109-2119, 2003.
30. Mathivanan S and Simpson RJ: ExoCarta: A compendium of exosomal proteins and RNA. Proteomics 9: 4997-5000, 2009.
31. Luftig M: Heavy LIFting: Tumor promotion and radioresistance in NPC. J Clin Invest 123: 4999-5001, 2013.
32. Ritty TM, Broekelmann TJ, Werneck CC and Mecham RP: Fibrillin-1 and -2 contain heparin-binding sites important for matrix deposition and that support cell attachment. Biochem J 375: 425-432, 2003.
33. Grass B, Wachtel M, Behnke S, Leuschner I, Niggli FK and Schäfer BW: Immunohistochemical detection of EGFR, fibrillin-2, P-cadherin and AP2beta as biomarkers for rhabdomyosarcoma diagnostics. Histopathology 54: 873-879, 2009.
34. Chandramouli A, Simundza J, Pinderhughes A and Cowin P: Choreographing metastasis to the tune of LTBP. J Mammary Gland Biol Neoplasia 16: 67-80, 2011.
35. Kim KW, Moretti L, Mitchell LR, Jung DK and Lu B: Endoplasmic reticulum stress mediates radiation-induced autophagy by perk-eIF2alpha in caspase-3/7-deficient cells. Oncogene 29: 3241-3251, 2010.
36. Fels DR, Ye J, Segan AT, Kridel SJ, Spiotto M, Olson M, Koong AC and Koumenis C: Preferential cytotoxicity of bortezomib toward hypoxic tumor cells via overactivation of endoplasmic reticulum stress pathways. Cancer Res 68: 9323-9330, 2008.
37. Rainger J, Keighren M, Keene DR, Charbonneau NL, Rainger JK, Fisher M, Mella S, Huang JT, Rose L, van't Hof R, *et al*: A *trans*-acting protein effect causes severe eye malformation in the *Mp* mouse. PLoS Genet 9: e1003998, 2013.
38. Thorpe C, Hoober KL, Raje S, Glynn NM, Burnside J, Turi GK and Coppock DL: Sulfhydryl oxidases: Emerging catalysts of protein disulfide bond formation in eukaryotes. Arch Biochem Biophys 405: 1-12, 2002.
39. Chakravarthi S, Jessop CE, Willer M, Stirling CJ and Bulleid NJ: Intracellular catalysis of disulfide bond formation by the human sulfhydryl oxidase, QSOX1. Biochem J 404: 403-411, 2007.
40. Pernodet N, Hermetet F, Adami P, Vejux A, Descotes F, Borg C, Adams M, Pallandre JR, Viennet G, Esnard F, *et al*: High expression of QSOX1 reduces tumorogenesis, and is associated with a better outcome for breast cancer patients. Breast Cancer Res 14: R136, 2012.
41. Yamaguchi H and Condeelis J: Regulation of the actin cytoskeleton in cancer cell migration and invasion. Biochim Biophys Acta 1773: 642-652, 2007.
42. Delorme V, Machacek M, DerMardirossian C, Anderson KL, Wittmann T, Hanein D, Waterman-Storer C, Danuser G and Bokoch GM: Cofilin activity downstream of Pak1 regulates cell protrusion efficiency by organizing lamellipodium and lamella actin networks. Dev Cell 13: 646-662, 2007.
43. Wang Y, Kuramitsu Y, Ueno T, Suzuki N, Yoshino S, Iizuka N, Zhang X, Oka M and Nakamura K: Differential expression of up-regulated cofilin-1 and down-regulated cofilin-2 characteristic of pancreatic cancer tissues. Oncol Rep 26: 1595-1599, 2011.
44. Kuramitsu Y, Wang Y, Okada F, Baron B, Tokuda K, Kitagawa T, Akada J and Nakamura K: Malignant progressive tumor cell clone exhibits significant up-regulation of cofilin-2 and 27-kDa modified form of cofilin-1 compared to regressive clone. Anticancer Res 33: 3661-3665, 2013.
45. Le AP, Huang Y, Pingle SC, Kesari S, Wang H, Yong RL, Zou H and Friedel RH: Plexin-B2 promotes invasive growth of malignant glioma. Oncotarget 6: 7293-7304, 2015.
46. Jia P, Liu Y and Zhao Z: Integrative pathway analysis of genome-wide association studies and gene expression data in prostate cancer. BMC Syst Biol 6 (Suppl 3): S13, 2012.
47. Codogno P: Autophagy in cell survival and death. J Soc Biol 199: 233-241, 2005 (In French).
48. Oswald J, Boxberger S, Jørgensen B, Feldmann S, Ehninger G, Bornhäuser M and Werner C: Mesenchymal stem cells can be differentiated into endothelial cells in vitro. Stem Cells 22: 377-384, 2004.
49. Foster LJ, Zeemann PA, Li C, Mann M, Jensen ON and Kassem M: Differential expression profiling of membrane proteins by quantitative proteomics in a human mesenchymal stem cell line undergoing osteoblast differentiation. Stem Cells 23: 1367-1377, 2005.
50. Behnan J, Isakson P, Joel M, Cilio C, Langmoen IA, Vik-Mo EO and Badn W: Recruited brain tumor-derived mesenchymal stem cells contribute to brain tumor progression. Stem Cells 32: 1110-1123, 2014.
51. Burns JS, Abdallah BM, Guldberg P, Rygaard J, Schrøder HD and Kassem M: Tumorigenic heterogeneity in cancer stem cells evolved from long-term cultures of telomerase-immortalized human mesenchymal stem cells. Cancer Res 65: 3126-3135, 2005.
52. Dalerba P, Dylla SJ, Park IK, Liu R, Wang X, Cho RW, Hoey T, Gurney A, Huang EH, Simeone DM, *et al*: Phenotypic characterization of human colorectal cancer stem cells. Proc Natl Acad Sci USA 104: 10158-10163, 2007.
53. Moon BS, Jeong WJ, Park J, Kim TI, Min S and Choi KY: Role of oncogenic K-Ras in cancer stem cell activation by aberrant Wnt/β-catenin signaling. J Natl Cancer Inst 106: djt373, 2014.
54. Yan M, Yang X, Wang L, Clark D, Zuo H, Ye D, Chen W and Zhang P: Plasma membrane proteomics of tumor spheres identify CD166 as a novel marker for cancer stem-like cells in head and neck squamous cell carcinoma. Mol Cell Proteomics 12: 3271-3284, 2013.
55. Nowell PC: The clonal evolution of tumor cell populations. Science 194: 23-28, 1976.
56. Reya T, Morrison SJ, Clarke MF and Weissman IL: Stem cells, cancer, and cancer stem cells. Nature 414: 105-111, 2001.